


Predicting the Effects of Climate Change on Dengue Vector Densities in Southeast Asia through Process-Based Modeling

Lucas Bonnin,¹  Annelise Tran,^{2,3,4,5} Vincent Herbreteau,^{6,7} Sébastien Marcombe,⁸ Sébastien Boyer,⁹ Morgan Mangeas,¹ and Christophe Menkes¹

¹ENTROPIE (UMR 9220), IRD, Université de la Réunion, CNRS, Ifremer, Université de Nouvelle Calédonie, Nouméa, Nouvelle-Calédonie

²CIRAD, UMR TETIS, Sainte-Clotilde, Reunion Island, France

³TETIS, Université Montpellier, AgroParisTech, CIRAD, CNRS, INRAE, Montpellier, France

⁴CIRAD, UMR ASTRE, Sainte-Clotilde, Reunion Island, France

⁵ASTRE, Université Montpellier, CIRAD, INRAE, Montpellier, France

⁶ESPACE-DEV, IRD, Université Antilles, Université Guyane, Université Montpellier, Université de la Réunion, Montpellier, France

⁷ESPACE-DEV, IRD, Université Antilles, Université Guyane, Université Montpellier, Université de la Réunion, Phnom Penh, Cambodia

⁸Medical Entomology and Vector-Borne Disease Laboratory, Institut Pasteur du Laos, Vientiane, Lao PDR

⁹Medical and Veterinary Entomology Unit, Institut Pasteur du Cambodge, Phnom Penh, Cambodia

BACKGROUND: *Aedes aegypti* and *Ae. albopictus* mosquitoes are major vectors for several human diseases of global importance, such as dengue and yellow fever. Their life cycles and hosted arboviruses are climate sensitive and thus expected to be impacted by climate change. Most studies investigating climate change impacts on *Aedes* at global or continental scales focused on their future global distribution changes, whereas a single study focused on its effects on *Ae. aegypti* densities regionally.

OBJECTIVES: A process-based approach was used to model densities of *Ae. aegypti* and *Ae. albopictus* and their potential evolution with climate change using a panel of nine CMIP6 climate models and climate scenarios ranging from strong to low mitigation measures at the Southeast Asian scale and for the next 80 y.

METHODS: The process-based model described, through a system of ordinary differential equations, the variations of mosquito densities in 10 compartments, corresponding to 10 different stages of mosquito life cycle, in response to temperature and precipitation variations. Local field data were used to validate model outputs.

RESULTS: We show that both species densities will globally increase due to future temperature increases. In Southeast Asia by the end of the century, *Ae. aegypti* densities are expected to increase from 25% with climate mitigation measures to 46% without; *Ae. albopictus* densities are expected to increase from 13%–21%, respectively. However, we find spatially contrasted responses at the seasonal scales with a significant decrease in *Ae. albopictus* densities in lowlands during summer in the future.

DISCUSSION: These results contrast with previous results, which brings new insight on the future impacts of climate change on *Aedes* densities. Major sources of uncertainties, such as mosquito model parametrization and climate model uncertainties, were addressed to explore the limits of such modeling. <https://doi.org/10.1289/EHP11068>

Introduction

Mosquitoes from the genus *Aedes* are major vectors for several human arboviruses of global importance, such as dengue, Zika, and Chikungunya viruses.^{1–3} These viruses can cause severe febrile diseases with long-term physical and cognitive consequences. Due to their widespread distribution and the large populations at risk, they represent a major burden on global health and are estimated to be responsible annually for millions of disability-adjusted life years (DALY⁴). Because no specific treatment exists for such viral diseases, with the exception of dengue, for which the World Health Organization recommends the use of vaccine in very specific cases only,⁵ vector surveillance and control represent the only available and effective strategy to mitigate the outbreaks of these diseases.^{6–9} Indeed, vector density is a major component of vectorial capacity¹⁰ and potentially plays a key role in the transmission of arboviruses, notably for dengue

fever.^{11–16} Mosquito life cycles are highly dependent on weather conditions because temperature drives reproduction, maturation and mortality,¹⁷ whereas rainfall drives the availability of breeding sites¹⁸ and juvenile mortality (washing off of aquatic stages). As a result, mosquito densities are expected to be greatly impacted by global climate change, but it remains unclear how and where vector risk will change in the future.

Predicting the future evolution of vector risk relies on large spatial scale modeling of *Aedes* population dynamics in response to climate spatial and temporal variations. Species distribution models have been developed for the two main dengue vector species, *Ae. aegypti* and *Ae. albopictus*, to predict the future response of these species' distribution to climate change at global or continental scales.^{19–22} Such statistical models bring valuable knowledge about the potential ecological niche of the associated vectorborne diseases, yet they cannot bring insight about the level of vector risk in regions where these species are already present all year long. Statistical modeling of mosquito population densities, however, poses a greater challenge due to the difficulty to gather large data sets of spatially consistent density observations to effectively build the models.

Although data are key to constructing statistical models, mechanistic approaches on the other hand are less impacted by data availability because data are usually only used for validation. Such mechanistic models can simulate mosquitoes' life cycles based on quantified knowledge of the response of their different life stages to climate variations. Process-based models have successfully been employed to describe *Aedes* mosquitoes' density variations at local and global scales.^{23–25} However, they were seldom applied to climate projections to predict the future evolution of vector risk. To date, a single study used mechanistic models to

Address correspondence to Lucas Bonnin, ENTROPIE (UMR 9220), IRD, Université de la Réunion, CNRS, Ifremer, Université de Nouvelle Calédonie, Nouméa, Nouvelle-Calédonie. Email: lucasbonnin@hotmail.fr

Supplemental Material is available online (<https://doi.org/10.1289/EHP11068>).

The authors declare they have nothing to disclose.

Received 8 February 2022; Revised 19 September 2022; Accepted 21 October 2022; Published 6 December 2022.

Note to readers with disabilities: *EHP* strives to ensure that all journal content is accessible to all readers. However, some figures and Supplemental Material published in *EHP* articles may not conform to 508 standards due to the complexity of the information being presented. If you need assistance accessing journal content, please contact ehpsubmissions@niehs.nih.gov. Our staff will work with you to assess and meet your accessibility needs within 3 working days.

predict the future evolution of densities of one *Aedes* species, *Ae. aegypti*, at a global scale,²⁵ but with no validation of temporal dynamics. Because such models rely on strong hypotheses about mechanistic processes, confidence in future predictions can only arise from the comparison and confrontation of results from independently built models or independent data.

In this study, a compartment process-based model was used to describe seasonal variations of densities of two *Aedes* mosquito species, *Ae. aegypti* and *Ae. albopictus*, in response to contemporary and future climates. *Aedes* densities were modeled on a 10 by 10 arc-minutes grid at a regional scale in Southeast Asia (SEA), where both species are ubiquitous and where *Aedes*-borne diseases (especially dengue fever) display frequent outbreaks and pose crucial public health concerns.^{26–30} To validate the model seasonal dynamics, we used original density data from temporal entomological surveys from two Southeast Asian cities: Phnom Penh, Cambodia, and Vientiane, Lao People's Democratic Republic (here after Lao PDR). Based on climate projections from a range of climate models and scenarios of greenhouse gas emissions (Worldclim database³¹; <https://www.worldclim.org/data/index.html>), predictions about the evolution of densities of both species were mapped over selected future periods of the 21st century.

Our results were used to both discuss the potential vector evolutions with the diversity of future potential climates but also the advantages and flaws of mechanistic approaches in comparison with other statistical modeling. Overall, the framework allows us to discuss the magnitudes of predictions uncertainties, which are key to identify future improvements.

Methods

Study Area

The study area includes the Southeast Asian countries of Myanmar, Lao PDR, Thailand, Cambodia, and Vietnam, whose latitudes varies between 5.6° and 28.5° North. This region is characterized by a contrasting topography, with lowlands under 300 m in altitude (in central Myanmar, Thailand, Cambodia, and southern and northern Vietnam) and highlands in the north part of the region (in eastern Myanmar, northern Thailand, Lao PDR, and northern Vietnam) (Figure S1). The coldest months in the region (December, January, February) are characterized by average temperatures between 16°C and 24°C, whereas during the warmest months (April, May, June), they vary between 24°C and 28°C. Rains show a strong seasonality in the region, with the rainy season roughly occurring between May and October, with precipitations averaging 8 mm/d and reaching 40 mm/d in some parts of the region (e.g., western Myanmar).

Process-Based Climate-Driven Model

Mosquito population dynamics were modeled through a process-based approach, using the general mechanistic framework proposed by Cailly et al.³² This framework describes, through a system of ordinary differential equations (ODE), variations of mosquito abundance in 10 compartments, corresponding to different stages of mosquito life cycle. Aquatic stages are divided into eggs (*E*), larvae (*L*), and pupae (*P*); adult stages are divided into emerging (*A_{em}*), nulliparous (*A₁*), and parous females (*A₂*). Nulliparous and parous females are then subdivided according to their behavior: host seeking (*A_h*), transition from engorged to gravid (*A_g*), and oviposition site seeking (*A_o*). This framework was later used to develop models of *Ae. albopictus* population dynamics in temperate³³ and tropical climates.³⁴ In this study, the

ODE system from Tran et al.³⁴ was used to model population dynamics of both species separately.

$$\begin{cases} \dot{E} = \gamma_{Ao}(\beta_1 A_{1o} + \beta_2 A_{2o}) - (m_E + f_E)E \\ \dot{L} = f_E E - (m_L(1 + L/k_L) + f_L)L \\ \dot{P} = f_L L - (m_P + f_P)P \\ \dot{A}_{em} = f_P P \sigma e^{-\mu_{em}(1 + P/k_P)} - (m_A + \gamma_{Aem})A_{em} \\ \dot{A}_{1h} = \gamma_{Aem} A_{em} - (m_A + \mu_r + \gamma_{Ah})A_{1h} \\ \dot{A}_{1g} = \gamma_{Ah} A_{1h} - (m_A + f_{Ag})A_{1g} \\ \dot{A}_{1o} = f_{Ag} A_{1g} - (m_A + \mu_r + f_{Ao})A_{1o} \\ \dot{A}_{2h} = f_{Ao}(A_{1o} + A_{2o}) - (m_A + \mu_r + \gamma_{Ah})A_{2h} \\ \dot{A}_{2g} = \gamma_{Ah} A_{2h} - (m_A + f_{Ag})A_{2g} \\ \dot{A}_{2o} = f_{Ag} A_{2g} - (m_A + \mu_r + \gamma_{Ao})A_{2o} \end{cases}$$

The diagram of the model is available in Figure S2. All parameters and functions are derived from results of experimental studies.^{35,36} In this study, we used the *Ae. albopictus* parameters and functions described in Tran et al.³⁴ and *Ae. aegypti* parameters and functions gathered from literature.^{23,37}

Parameter values are described in Table 1, adapted from Tran et al.³⁴: for each stage *X*, γ_X is the transition rate to the next compartment, μ_X is the mortality rate, β_X is the egg laying rate, and σ is the sex ratio at the emergence; μ_r is an additional adult mortality rate related to seeking behavior.

Functions are used to describe the temperature- and precipitation-dependent transition rates (f_X), mortality rates (m_X), and carrying capacities (k_X), which vary over time (Table 2). Carrying capacity is driven by precipitation and is used to regulate the density-dependent mortality of aquatic stages (larvae and pupae): As rainfall fills breeding sites, higher precipitation enables higher larval and pupal densities before high mortality.

The population dynamics of both species were modeled on a 10 arc-minutes grid (about 16.3 km in the north of Myanmar and 18.4 km in the south of Thailand), based on the spatial resolution of climate data. Each grid cell was considered as independent from the others.

Climate Data

Population dynamics were modeled using seasonal variations of climate variables (surface air temperatures and precipitation) from contemporary data and from climate models using future projections. These data were obtained from the WorldClim initiative³¹ (<https://www.worldclim.org/>) at a monthly scale. As the model uses daily inputs, climate data were interpolated linearly to obtain daily values.

The contemporary seasonal climate corresponded to the 1970–2000 period. Future projections were based on nine climate models (BCC-CSM2-MR,³⁸ CNRM-CM6-1,³⁹ CNRM-ESM2-1,⁴⁰ CanESM5,⁴¹ GFDL-ESM4,⁴² IPSL-CM6A-LR,⁴³ MIROC-ES2L,⁴⁴ MIROC6,⁴⁵ and MRI-ESM2-0⁴⁶) for four scenarios of greenhouse gas emissions (Shared Socioeconomic Pathways: SSP1 2.6, SSP2 4.5, SSP3 7.0, and SSP5 8.5, based on CMIP6) and for four periods (2021–2040, 2041–2060, 2061–2080, 2081–2100) at a 10 arc-minutes spatial resolution. Special focus was given on climate projections following SSP1 2.6 and SSP3 7.0 because they correspond respectively to the objectives set by the Paris Agreements and to a most realistic scenario of greenhouse gas emissions in the absence of strong mitigation, as currently experienced. To be more specific, SSP1 2.6 corresponds to a zero-emission target reached after 2050, whereas SSP3 7.0 corresponds to a steady increase in greenhouse gas emissions throughout the century, with CO₂ emissions in the year 2100 twice as high as contemporary levels. In Southeast Asia, at the end of the century, SSP1 2.6 and SSP3 7.0 are predicted to

Table 1. Process-based model parameters.

Notation	Definition	Value	
		<i>Ae. albopictus</i>	<i>Ae. aegypti</i>
β_1	Number of eggs laid/ovipositing nulliparous female		60.0
β_2	Number of eggs laid/ovipositing parous female		80.0
σ	Sex ratio at emergence		0.5
γ_{Aem}	Development rate of emerging adults (per day)		0.4
γ_{Ah}	Transition rate from host-seeking to engorged adults (per day)		0.2
γ_{Ao}	Minimum transition rate from ovipositing to host-seeking adults (per day)		0.2
μ_E	Minimum egg mortality rate (per day)	0.05	0.01
μ_{em}	Mortality rate during emergence (per day)		0.1
μ_r	Mortality rate related to seeking behavior (per day)		0.08
T_E	Minimal temperature needed for egg development	10.0	
TDD_E	Total number of degree days necessary for egg development (°C.day)	110	
T_{Ag}	Minimal temperature needed for egg maturation in females (°C)	10.0	
TDD_{Ag}	Total number of degree days necessary for egg maturation in females (°C.day)	77.0	

Note: Adapted from Table 2 from Tran et al.³⁴

result in an average increase of temperature of 1.5°C and 3.5°C, respectively, and an average increase of precipitation of 0.2 and 0.1 mm/d, respectively, although with high seasonal and spatial heterogeneity (Figure S7). Note that results for other scenarios are also given but discussed more briefly.

All simulations were run during 2 successive climatological years, but only the last year was analyzed to discard the model spin-up occurring during the first year. Monthly mean outputs were considered for the rest of the analysis.

Analysis and Mapping

To assess the relative increase or decrease of adult female densities associated with each climate projection, a percentage change was computed as the ratio of future density over contemporary density.

To assess the concordance between projections associated with the nine climate models, one Student's *t*-test was performed in each grid cell over the nine percentage change values to test for a significant difference of their mean from zero (H_0 : percentage change is equal to zero, H_1 : percentage change is different from zero). Statistical significance (*p*) was set at the 5% level.

Although the compartment model allows studying the temporal dynamics of the *Aedes* species, it requires an *a priori* knowledge of the potential mosquito presence, such as the dynamics given by species distribution models. Hence, to produce realistic contemporary mosquito density maps, we first built spatial species distribution for the two species in the region. Such distributions consisted of spatial predictions of probability of occurrence of each species, computed from species distribution models (SDMs) based on occurrence data from Kraemer et al.²⁰ and topography and land cover data (see Figure S3A for such species distributions). Details about the SDM are provided in the "Species Distribution Modeling" section. These maps were then used to weight the contemporary simulations of species spatial densities given by the mosquito dynamical model. These weighted densities maps were then linearly scaled to vary between 0 and 1 to produce a simple and interpretable index of density.

It has to be noted that future percentage changes relied only on climate variations and on the process-based model. Indeed, the SDM weighting was only based on topography and current contemporary land cover data (no future projections of land cover were used); its effect thus did not appear in the final ratio describing density percentage change.

Species Distribution Modeling

Geographical distribution of both species was modeled in the study area based on occurrence data and land-cover and topography maps. Occurrence data for both species were obtained from Kraemer

et al.²⁰ and subsampled over the two countries of the region with the largest available data, Thailand and Vietnam, resulting in a data set of 102 occurrences for *Ae. albopictus* and 725 occurrences for *Ae. aegypti* (Figure S3A). For both species, the same number of pseudo-absences was randomly sampled in both countries. Land cover data from the FROM-GLC initiative (Finer Resolution Observation and Monitoring – Global Land Cover)⁴⁷ and topography data from the Shuttle Radar Topography Mission (SRTM)⁴⁸ were used as independent variables. Land cover data consisted in a classification of land surface in eight categories (cropland, forest, grassland, shrubland, wetland, water, impervious surface, and bare land) at a spatial resolution of 10 m. Because occurrence data was available on a 0.01-degree grid, land cover data were converted to this scale by computing proportions of each land cover category in each grid cell. Topography data was available at a 90 m spatial resolution but converted to 0.01° by computing elevation and slope averages and variability of slope in each grid cell.

An ensemble modeling approach was used to model presence/absence as dependent on land cover and topography. Ensemble modeling was performed using the *biomod2* R package (version 4.0.3; R Development Core Team), considering a combination of generalized linear modeling (GLM), gradient boosting modeling (GBM), classification tree analysis (CTA), artificial neural network (ANN), flexible discriminant analysis (FDA) and random forest (RF) to compute spatial predictions of probability of observation. Individual model quality was assessed through a 5-fold cross-validation process and area under the receiver operating characteristic curve (ROC AUC) quality metrics. All models with AUC values <0.85 were discarded (Table S1); next, the predictions of the remaining models were averaged with weights proportional to their AUC to compute a single prediction at a 0.01° resolution over the entire study area (Figure S3A). The resulting distribution maps were then converted to match the 10-minutes-of-arc grid used to compute simulations from the process-based climate-driven model. Distribution maps were thus used to weight the contemporary simulations of species spatial densities given by this process-based model, as previously described.

Process-Based Model Sensitivity to Climate Variables

A posteriori sensitivity of modeled species to temperature and precipitation was estimated as follows: 10,000 combinations of 100 constant values of temperature (between 10° and 40°C), and 100 constant values of precipitation (between 0 and 20 mm/d) were used to simulate the evolution of mosquito density over 30 d. Mosquito density values at the end of these 30 d were then mapped as a function of temperature and precipitation, allowing a

Table 2. Process-based model functions.

Notation	Definition	Expression	
		<i>Ae. Albopictus</i>	<i>Ae. Aegypti</i>
f_E	Transition function from egg to larva	$\begin{cases} \frac{T - T_E}{TDD_E} & \text{if } T > T_E \\ 0 & \text{otherwise} \end{cases}$	$\frac{24\rho \frac{T^K}{298} e^{\frac{\Delta H_A}{R}(\frac{1}{298} - \frac{1}{T^K})}}{1 + e^{\frac{\Delta H_H}{R}(\frac{1}{T_{1/2H}} - \frac{1}{T^K})}}$ With $\rho = 0.01066$; $\Delta H_A = 10,798.18$; $\Delta H_H = 100,000$; $T_{1/2H} = 14,184.5$
f_L	Transition function from larva to pupa	$q_1 T^2 + q_2 T + q_3$ with $q_1 = -0.0007$; $q_2 = 0.0392$; $q_3 = -0.3911$	$\frac{24\rho \frac{T^K}{298} e^{\frac{\Delta H_A}{R}(\frac{1}{298} - \frac{1}{T^K})}}{1 + e^{\frac{\Delta H_H}{R}(\frac{1}{T_{1/2H}} - \frac{1}{T^K})}}$ With $\rho = 0.00873$; $\Delta H_A = 26,018.51$; $\Delta H_H = 55,990$; $T_{1/2H} = 304.58$
f_P	Transition function from pupa to emerging adult	$q_1 T^2 + q_2 T + q_3$ with $q_1 = -0.0008$; $q_2 = 0.0051$; $q_3 = -0.319$	$\frac{24\rho \frac{T^K}{298} e^{\frac{\Delta H_A}{R}(\frac{1}{298} - \frac{1}{T^K})}}{1 + e^{\frac{\Delta H_H}{R}(\frac{1}{T_{1/2H}} - \frac{1}{T^K})}}$ With $\rho = 0.0161$; $\Delta H_A = 14,931.94$; $\Delta H_H = -472,379$; $T_{1/2H} = 148.45$
f_{Ag}	Transition function from engorged adult to ovipositing site-seeking adult	$\frac{T - T_{Ag}}{TDD_{Ag}}$	$\frac{24\rho \frac{T^K}{298} e^{\frac{\Delta H_A}{R}(\frac{1}{298} - \frac{1}{T^K})}}{1 + e^{\frac{\Delta H_H}{R}(\frac{1}{T_{1/2H}} - \frac{1}{T^K})}}$ With $\rho = 0.00898$; $\Delta H_A = 15,725.23$; $\Delta H_H = 1,756,481.07$; $T_{1/2H} = 447.17$
f_{Ao}	Transition function from ovipositing to host-seeking adult		$\gamma_{Ao} \times (1 + P_{\text{norm}})$
m_E	Egg mortality		$\mu_E + \begin{cases} 0.1 & \text{if } P > 80 \\ 0 & \text{otherwise} \end{cases}$
m_L	Larva mortality		$0.02 + 0.0007e^{0.1838(T-10)} + \begin{cases} 0.5 & \text{if } P > 80 \\ 0 & \text{otherwise} \end{cases}$
m_P	Pupa mortality		$0.02 + 0.0003e^{0.2228(T-10)} + \begin{cases} 0.5 & \text{if } P > 80 \\ 0 & \text{otherwise} \end{cases}$
m_A	Adult mortality		$0.025 + 0.0003e^{0.1745(T-10)}$
k_L	Carrying capacity for larvae		$k_L = P_{\text{norm}}$
k_P	Carrying capacity for pupae		$k_P = P_{\text{norm}}$

Note: Adapted from Table 3 in Tran et al.³⁴ Transition and mortality rates and carrying capacity as a function of daily temperature (T) and precipitation (P). P_{norm} is the precipitation amount summed over a 1-wk period and normalized to vary between 0 and 1.

mean view of the modeled vector densities sensitivity to both temperature and precipitation.

Validation of Contemporary Temporal Dynamics

Entomological survey data from Phnom Penh and Vientiane were used to estimate the seasonal dynamics of *Ae. albopictus*

and *Ae. aegypti* densities. In Phnom Penh, surveys consisted in the sampling of 40 pagodas in the city (Figure S4), using 5 ovitraps per pagoda picked up every 8 wk between March 2019 and February 2020, resulting in 1,033 sampling points. Ovitrap without filter paper (black buckets)⁴⁹ were used to collect immature stages (larvae), which were then emerged in laboratory for species identification using morphological characters.⁵⁰

For each pagoda and each month, the proportion of emerged adults among collected larvae was used to extrapolate a number of captured larvae of each species. Extrapolated numbers of captured larvae were then standardized by pagoda (divided by the pagoda maximum) to account for differences in species abundance level between pagodas. In Lao PDR, surveys consisted in the sampling of five villages from the Vientiane province, using two to four BG sentinel traps per village picked up every 2 wk between May 2016 and March 2020 (Figure S4), resulting in 440 sampling points. Collected mosquitoes were identified using morphological characters.⁵⁰

Total numbers of captures of *Ae. albopictus* and *Ae. aegypti*, standardized by the corresponding number of traps, were computed in both cities and compared to standardized seasonal dynamics of densities simulated in these cities based on the local contemporary climate. Simulated densities were standardized using a multiplicative coefficient so that simulation and recorded curves had the same AUC.

Results

Model outputs based on contemporary seasonal variations of temperature and precipitations were compared to seasonal variations of density recorded from field surveys in Phnom Penh and Vientiane (Figure 1). In Phnom Penh, entomological field surveys showed seasonal dynamics of *Aedes* densities consisting in two peaks of density in June and October for *Ae. aegypti* and a consistent rising trend from March to October, followed by a rapid decrease for *Ae. albopictus*. In Vientiane, entomological surveys showed a less complex, one-peak symmetric seasonal dynamics of densities of both species. The model seasonal predictions captured the dynamics observed in both cities and for both species: the single-peak seasonal dynamics of both species in Vientiane and the more complex two-peak seasonal dynamics of *Ae. aegypti* and symmetric single-peak seasonal dynamics of *Ae. albopictus* in Phnom Penh. Precipitation was clearly the main driver of these dynamics, because it presented the same two-peak asymmetrical seasonality in Phnom Penh and one-peak symmetrical seasonality in Vientiane (Figure S5).

The model was then used to compute seasonal variations of *Ae. albopictus* and *Ae. aegypti* densities at continental scale in Southeast Asia, using the gridded contemporary observations and climate model future projections of temperature and precipitation (see Figures S6–S9). In the following, summer and winter refer to warmest and coldest trimesters in the region, corresponding respectively to April–May–June and December–January–February.

During summer months, *Ae. aegypti* showed elevated densities in lowlands and coastal areas (Figure 2), a spatial structure driven by its association to urban habitat (Figures S3B–C). This pattern contrasted with wintertime when *Ae. aegypti* densities were much lower over the domain due to lower temperature and precipitation (Figure S6).

For both SSP1 2.6 and SSP3 7.0 future climates, our model predicted that the *Ae. aegypti* densities would mostly increase in comparison with contemporary levels, except for a slight decrease in central Myanmar, northern Thailand, and Cambodia between April and May following SSP3 7.0 at the end of the century (Figure 2; Figure S9). Summer density evolution showed higher increases in the northern part of the domain, whereas winter densities showed stronger increases in the southern part of the domain, with increases reaching up to 100% for SSP3 7.0 and still 60% for SSP1 2.6 at the end of the century (Figure 2). These seasonal density increases were mostly driven by future temperature increases (Figure S10). Relative increases in densities in both winter and summer accentuated later in the century, most notably in the business-as-usual scenario SSP3 7.0, except in northern Myanmar during the winter months, where SSP1 2.6 resulted in higher densities than SSP3 7.0 (Figure 2).

Contemporary densities of *Ae. albopictus* were globally similar to *Ae. aegypti*, with maxima densities occurring during summer–autumn regionally (Figure 2; Figure S8) due to higher temperature and precipitation during these months. As for future *Ae. aegypti* evolutions, *Ae. albopictus* showed an increase in densities during the winter months in all climate scenarios (Figure 2; Figure S9), reaching +50% in 2041–2060 and up to +100% in 2081–2100 for the business-as-usual scenario (SSP3 7.0). In contrast to the trends of *Ae. aegypti* during summer months, *Ae. albopictus* showed marked dipoles of increasing and decreasing

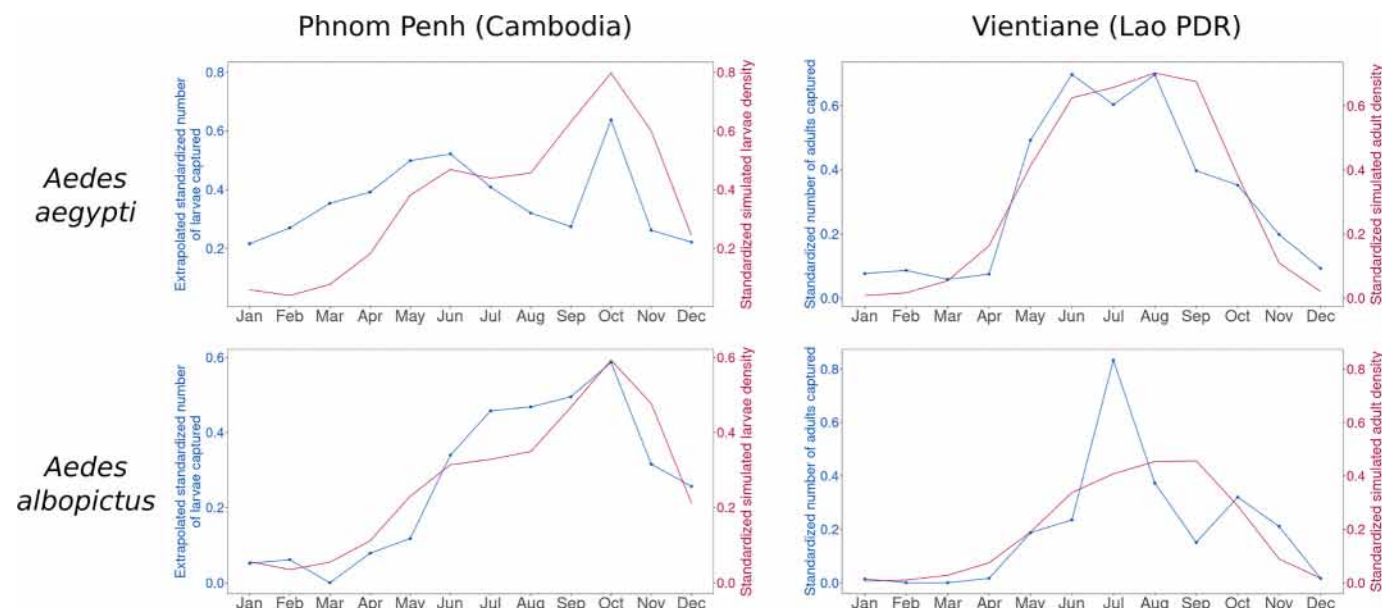


Figure 1. Comparison of temporal dynamics of simulated and recorded *Ae. albopictus* and *Ae. aegypti* adult female densities in Phnom Penh, Cambodia, and Vientiane, Lao PDR. Blue dotted lines correspond to monthly standardized captures of *Ae. aegypti* (top panels) and *Ae. albopictus* (bottom panels) from entomological surveys in Phnom Penh (left panels) and Vientiane (right panels). Red lines without dots represent monthly standardized simulated densities of both species, extracted from grid cells corresponding to Phnom Penh and Vientiane locations.

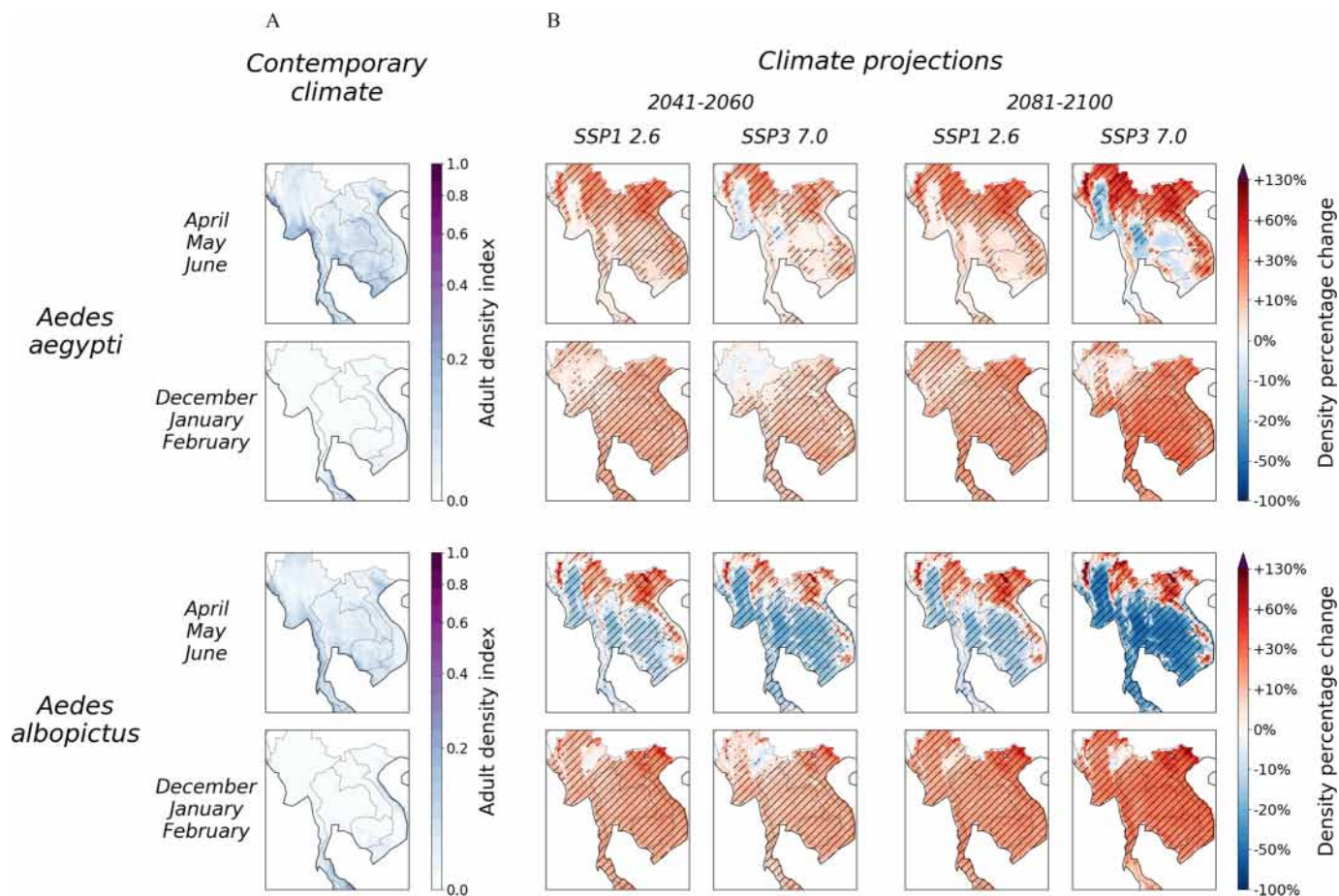


Figure 2. Modeled *Ae. albopictus* and *Ae. aegypti* adult female densities in Southeast Asia, based on contemporary climate and future projections. Panels A describe the spatial variations of modeled *Aedes* adult female density (top: *Ae. albopictus*; bottom: *Ae. aegypti*) for summer (April, May, June) and winter months (December, January, February), based on topography and land cover and on contemporary climate data input. Panels B describe projections of modeled *Aedes* adult female density in summer and winter months at the middle (2041–2060) and end of the century (2081–2100), based on future climate projections associated with the SSP1 2.6 and SSP3 7.0 emission scenarios. Percentage changes correspond to ratios of projected modeled density over contemporary modeled densities, averaged over the nine simulations associated with the nine climate models. Positive (red) and negative (blue) percentage changes correspond respectively to higher and lower predicted mosquito density in comparison with the contemporary situation. Purple grid cells correspond to percentage changes greater than a threshold of 130%, mostly corresponding to areas of null to low contemporary adult female density. Diagonal hashing represent grid cells where percentage changes associated with the nine climate models are significantly different from zero (Student's *t*-test, $p < 0.05$).

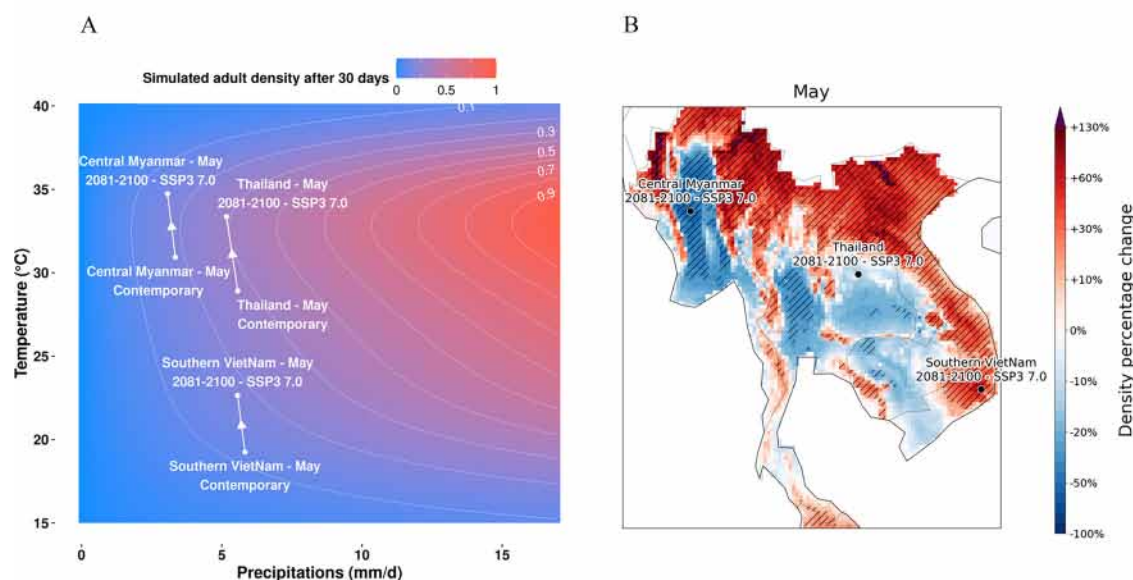
densities in the northern and southern parts of the continent, respectively (Figure 2; Figure S9), for all periods and climate scenarios. This contrasted pattern accentuated along the century (Figure S11) and with increased greenhouse gas emissions corresponding to decreased mitigation scenarios (Figure S12). The dipole accentuation corresponded to topographic constraints, with increased densities in highlands and decreased densities in lowlands (Figure S13).

The sensitivity of the process-based model to temperature and precipitation was estimated through 10,000 simulations of population dynamics across a range of temperature and precipitation values (Figure 3). Higher precipitation resulted in higher adult female densities for both species (Figures 3A,C). However, the model displayed an optimal temperature above which increasing temperatures resulted in lower adult female densities. This thermal optimum was much warmer for *Ae. aegypti* (33°C; Figure 3A) than for *Ae. albopictus* (29°C; Figure 3C). In the range of temperature and precipitation values used here to evaluate the sensitivity of the model, future changes in temperature were expected to be of greater importance on model outputs than future changes in precipitation. Indeed, temperature increases at the end of the century following the SSP3 7.0 scenario were shown to be relatively uniform within the domain and to reach as

much as 4.7°C (Figure S7), whereas changes in precipitation were usually projected to be weak and within -1 to $+1$ mm/d, only reaching -3.5 OR $+3.5$ mm/d in localized areas (e.g., south Myanmar in September; Figure S7). During summer months in southern Vietnam, rising temperatures predicted at the end of the century along the SSP3 7.0 scenario were thus expected to bring *Ae. aegypti* and *Ae. albopictus* closer to their thermal optimums (Figure 3A,C), resulting in an increase in densities (Figures 3B,D). In contrast, in central Myanmar, where contemporary temperatures are higher, a rise was expected to exceed thermal optimum of both species (Figures 3A,C), resulting in a decrease of densities (Figures 3B,D). In Thailand, rising temperatures were shown to have a contrasting effect on the two species, bringing *Ae. aegypti* closer to its thermal optimum (Figure 3A), resulting in an increase in densities (Figure 3B) and exceeding the optimum of *Ae. albopictus* (Figure 3C), which in turn led to a decrease in densities (Figure 3D).

Finally, Figure 4 summarizes the evolution of both *Aedes* species for the next century as a function of the four climate scenarios and for the two seasons in the highlands and lowlands (regions that were shown to show coherent evolutions). Because future changes in precipitation were shown to be globally null in both highlands and lowlands (Figure S14), future precipitation

Aedes aegypti



Aedes albopictus

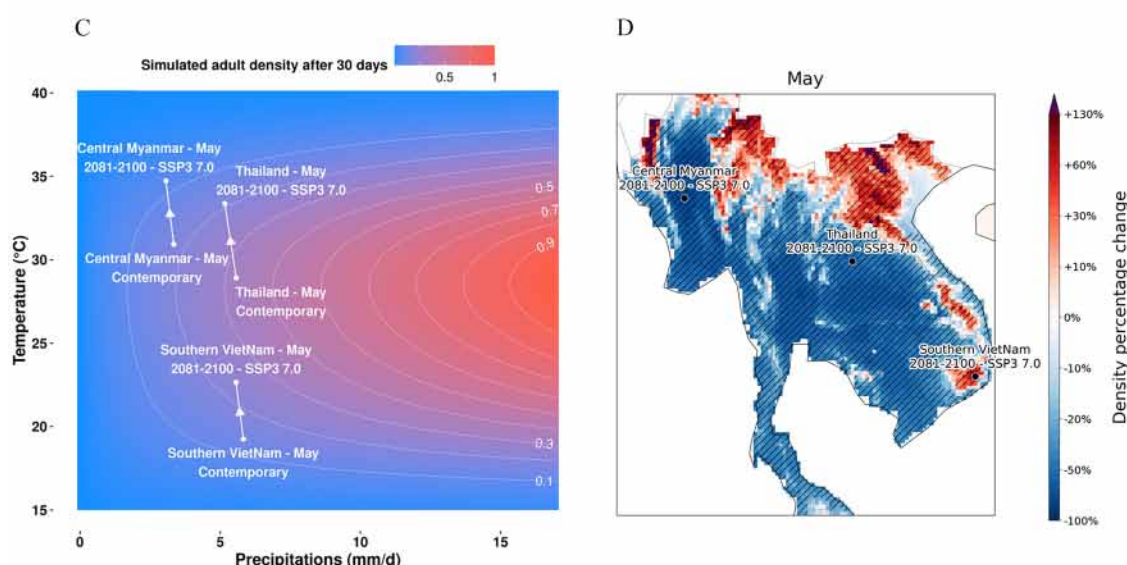


Figure 3. Process-based model sensitivity to temperature and precipitation. Process-based model simulations were performed over various constant values of temperature and precipitations. Model outputs were extracted after 30 d of simulation and plotted against corresponding temperature and precipitations (Panels A and C). White dots and arrows represent evolution of temperature and precipitations from contemporary to future projections (2081–2100/SSP3 7.0) at a specific month and location, displayed on the panels B and D. Note: SSP, Shared Socioeconomic Pathways.

had overall weak influences on the species' future evolution. By contrast, future changes in temperature were always positive and similar in both highlands and lowlands (Figure S14). The differing response of both species in highlands and lowlands during summer months, with a weaker rise in *Ae. aegypti* densities in lowlands in comparison with highlands (+5% and +33% at the end of the century for the SSP3 7.0) and a decrease in *Ae. albopictus* in lowlands (–24%; Figure 4), can be explained by warmer contemporary temperatures in lowlands. Indeed, a future rise in temperature in already warm lowlands is likely to result in *a*) a small increase in *Ae. aegypti* densities due to contemporary densities already close to their thermal optimum, and *b*) a decrease of *Ae. albopictus* densities due to

excessive heat bringing the species beyond its thermal optimum. In highlands during summer months and in the entire domain during winter months, rising temperatures resulted in an increase in densities of both species because their present-day background climate was well below the excessive heat thresholds. Indeed, at the end of the century following the SSP3 7.0, *Ae. aegypti* and *Ae. albopictus* densities increased by 15% and 21%, respectively, in the entire domain during winter months.

The potential effects of climate mitigation measures was investigated by computing the relative change in adult density associated with a transition from SSP3 7.0 to SSP1 2.6 at the end of the century. Over the entire domain, mitigation measures would result in an average yearly decrease in *Ae. aegypti* densities of 5% and

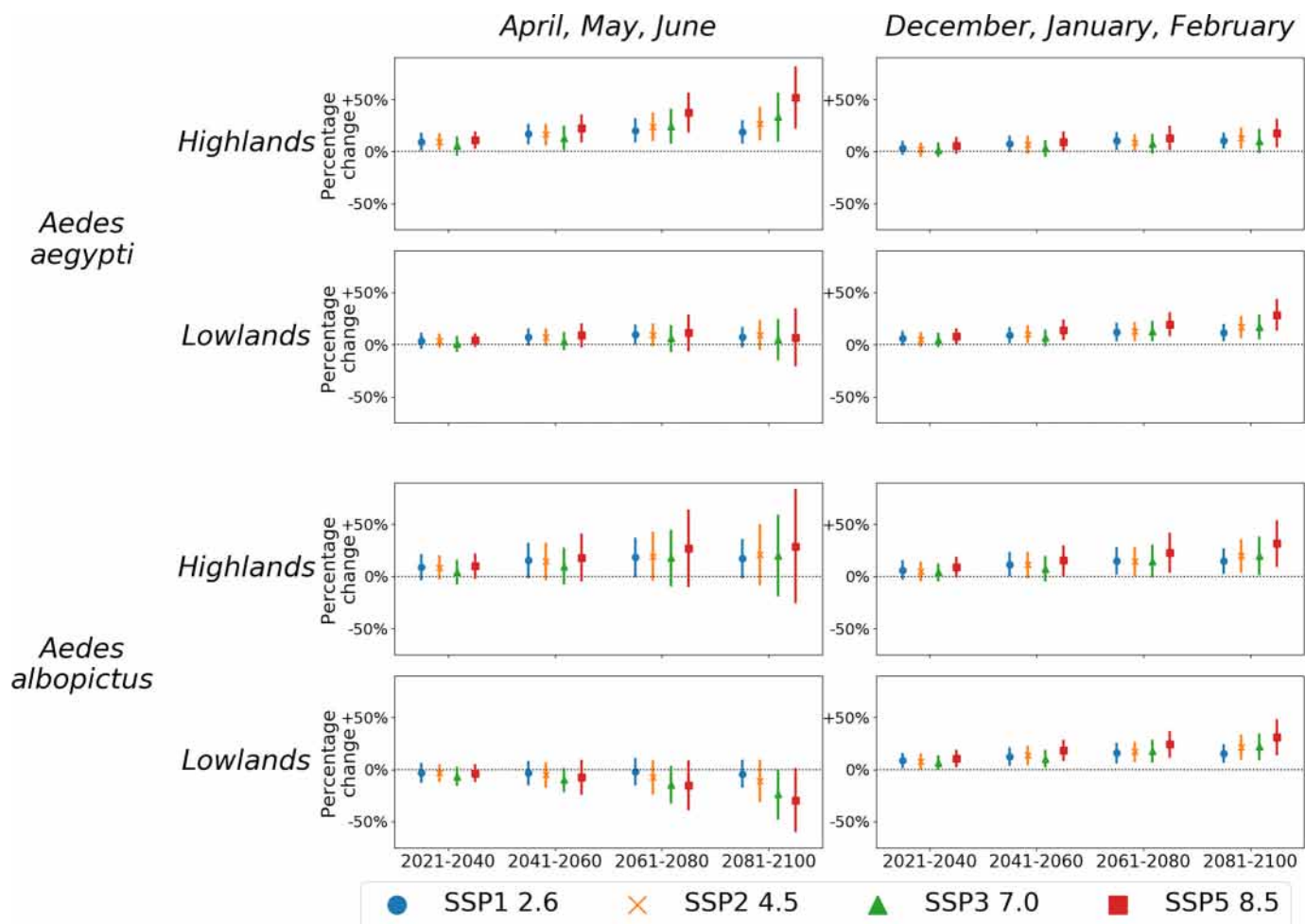


Figure 4. Evolution of projected *Aedes* density across the 21st century following four SSP scenarios. Grid cells were split in two groups considering their elevation (Highlands: elevation >600 m, Lowlands: elevation <600 m). For each species, scenario, period and month, points and bars represent respectively mean and standard deviation of percentage change values associated to all climate models and all grid cells. Note: SSP, Shared Socioeconomic Pathways.

an increase in *Ae. albopictus* densities of 7%. Such mitigation measures would even result in a global increase of *Ae. albopictus* densities of 28% during summer months, because colder temperatures would bring the species closer to its thermal optimum (Figure S15C and D). For *Ae. aegypti* during summer months, these mitigation measures would result in an average increase in densities of 2%, although with some local variations, e.g., increases of ~20%–40% in central Thailand and Myanmar and decreases of about 10%–20% in Vietnam and in the north of the domain (Figure S15B).

Discussion

Main Results

A process-based model was used here to simulate climate-dependent seasonal population dynamics of two human arbovirus vectors, *Ae. aegypti* and *Ae. albopictus*, in Southeast Asia, for present and future climates. Using climate model projections of temperature and precipitation enabled us to produce predictions of vector densities up to the end of the 21st century in four climate scenarios. Results suggest that densities of *Ae. aegypti* mosquitoes, which are currently the main vectors of dengue fever in Southeast Asia, will increase in most parts of the continent during the 21st century in all scenarios. Even strict implementation of the Paris Agreement's greenhouse gas emissions reductions [here, the SSP1 2.6, Intergovernmental Panel on Climate Change

(IPCC) report]^{51,52} would not mitigate this rise in mosquito densities. Indeed, following the SSP1 2.6 pathway instead of the current SSP3 7.0 would result in a very limited decrease in *Ae. aegypti* densities and even a slight increase in *Ae. albopictus* densities.

Given the current climate model projections, the projected changes of *Aedes* densities are more likely to be driven by a future change of temperature than a change in precipitation, which do not show clear evolutions between climate models. Indeed, although climate models systematically predict a rise of temperatures in all Southeast Asia, they do not agree in predicting the direction of the change in precipitation in most parts of the continent, especially during summer months (Figure S7). Given the agreement of the modeled temperature projections, and even with such precipitation uncertainties in state-of-the-art model CMIP6 outputs, mosquito densities modeled from all separate climate projections agreed in the direction of the future change of *Aedes* species, with an overall increase of *Ae. aegypti* densities and dipoles of increased and decreased *Ae. albopictus* densities in highlands and lowlands, respectively.

Implications of Rising Temperatures

Health implications. Because *Ae. aegypti* is the main vector of dengue fever in Southeast Asia, rising temperatures on the continent, along the current pathway where the SSP1 2.6 seems

unlikely and the SSP2 4.5/SSP3 7.0 seem more likely,⁵³ thus pose a real threat of increased dengue risk. Indeed, although relationships between vector indices and dengue risk are difficult to establish,¹¹ *Aedes* vector density has been shown to correlate positively with dengue occurrence.^{12–15} An increase of vector density, added to a lengthening of the season of high density (Figure S16) due to a lengthening of warmer seasons, are thus likely to result in higher incidence, higher numbers of outbreaks, and a lengthening of the epidemic season. Rising temperatures may also amplify this pattern through other mechanisms, such as an increase of *Aedes* feeding rate (up to a threshold of 36°C)^{54,55} or a reduction of the extrinsic incubation period, as it has been evidenced for dengue fever.^{54,56,57} Yet, the effects of rising temperatures on mosquitoes' densities may also be mitigated, because mosquitoes' life span may shorten with higher temperatures,^{35,37,55} reducing the risk of disease transmission between two hosts.^{58,59} Ryan et al. incorporated these complex biological factors into a global transmission model and provided future projections associated with various climate scenarios.⁶⁰ Their results in Southeast Asia align with ours, because they predicted an increase in disease transmission through *Ae. aegypti* as well as a reduction of transmission through *Ae. albopictus*. The same conclusions were reached in our study and in Ryan et al. about the effect of greenhouse gas emission mitigation measures, which were expected to attenuate transmission through *Ae. aegypti* but increase transmission through *Ae. albopictus*. Using various covariates including climate variables, Messina et al. built a statistical model of dengue occurrence at global scale to provide future predictions of climate change consequences on dengue risk.⁶¹ Their conclusions, however, contrast with ours in Southeast Asia, where they predict no real change in dengue risk in the future. These comparisons highlight the importance of considering models of different natures to reach scientific consensus and make reliable predictions about the health effects of climate change.

Ecology implications. Rising temperatures over the continent are likely to benefit *Ae. aegypti*, because the process-based model displays a high optimal temperature of 33.3°C (Figure 3). In contrast, rising temperatures are not expected to benefit *Ae. albopictus* in all of Southeast Asia, because the model displays a colder optimal temperature for this species at ~29.1°C (Figure 3), which is likely to be exceeded in most parts of Southeast Asia during summer months at the end of the century, according to all climate models. This factor resulted in the model predicting a decrease of *Ae. albopictus* densities everywhere except in the northern parts of Southeast Asia (Figure 2).

Regions where the model predicts rising *Ae. albopictus* densities match with topography maps and correspond to regions of higher altitude (Figure S13), where rising temperatures may get mosquitoes closer to their optimal temperature. This change could result in an expansion of the niche of the species toward higher altitudes, as has been projected in northern and southern America, Africa,^{19,62} and Asia.⁶³

An important consideration is that those overall optimal temperatures from the model were driven by the underlying temperature-dependent functions used to describe development and mortality rates of each life stage, based on the literature. For instance, the transition rate from larvae to pupae shows a lower optimal temperature for *Ae. albopictus* (28°C) than for *Ae. aegypti* (31°C; Figure S17). This factor, as well as considerations of climate variable uncertainties, naturally lead to the discussion on the potential limitations of this study.

Limitations. Outputs from the model provide only indices of the relative density of *Aedes* mosquitoes, but not quantitative evolutions of number of adults per surface area. To be able to provide such information, one needs to rely on the quantification

of the density of breeding sites, which is not available at this spatial scale from observations. Although relative indices of adult densities from the present modeling could provide valuable information on seasonal variability and future evolution, we advocate for a major effort in observations of breeding site adult densities on regional scales.

The two species were considered separately in our modeling framework, with no interaction between them. Yet, they can often share the same breeding sites and interspecific competition can occur among aquatic stages.^{64,65} For instance, both species can share the same breeding sites in urban environments (e.g., used tires).⁶⁶ Competition between *Aedes* species was not implemented in our framework because it depends on very complex mechanisms that could not be accurately described at this spatial scale, such as the diversity of breeding sites,⁶⁷ the nature of available nutrients,⁶⁵ and the history of species spread.⁶⁸ Our predictions about future changes in densities of each species should thus be interpreted as their separate response to changes in their climate suitability. Interspecific competition has the potential to increase or decrease our predictions for each species, for instance, in areas where they use similar breeding sites, such as urban areas.

Seasonal variations of densities were assessed using climate data at a monthly scale. This process did not allow us to account for the effects of extreme climate events occurring at a sub-monthly scale and responsible for extreme values of temperature or precipitation. For instance, extreme rainfall events can result in a drop in egg, larva, and pupa densities due to the washing of breeding sites, yet such mechanism could not be accounted for here due to the smoothing of monthly climate data. As pointed out in the IPCC reports,^{51,52} such extreme events are forecast to increase in the future and will need to be considered in future studies.

Considering the objective of asserting the impact of climate over *Aedes* densities, only rain-filled breeding sites were considered in the modeling framework. The presence of human-filled breeding sites (e.g., water storage containers, flower vases) typically found in urban settings where the SDM model predicts highest probabilities of occurrence (Figure S3B) could attenuate the effect of rainfall over density variations. Yet, we believe this is of negligible impact because urban settings also present numerous rain-filled artificial breeding sites, such as buckets, tires, and plastic bottles.^{69–71}

Although seasonal variability of mosquito density was assessed through the process-based model, its baseline spatial variability was estimated with statistical SDMs. SDMs predicted higher probability of presence in urban areas (high proportion of impervious surface land cover type) for both species. This pattern could be due to some extent to an observational bias in the occurrence database, with populated areas potentially more likely to be surveyed than rural areas. However, the potential observational bias is only pertinent when examining contemporary density maps but has no consequences for the conclusions about the future relative evolution of densities, which did not depend on SDM outputs. Still, SDM outputs could be pertinent to inform the future evolution of densities, for instance by using predictions of future urban expansion such as provided by Huang et al.⁷²

Several sources of uncertainty can, however, compromise future projections. First, the process-based model does not apprehend adaptive abilities of the species, potentially responsible for variations of biological responses to varying temperature, both on spatial scales with potentially differing genetic strains between regions^{73–75} and on evolutionary scale, with species likely to adapt to changing environmental conditions. Such a mechanism is

particularly relevant for *Aedes* species, considering the role of adaptation to cold temperatures in the recent invasion of *Ae. albopictus* in temperate regions, such as Europe and northern America.^{76,77}

Another source of uncertainty comes from the climate model data used as inputs in the process-based model. In our study, particular focus was given to projections corresponding to the SSP3 7.0, because it is considered as one likely scenario if current greenhouse gas emissions are not curbed drastically to reach the levels in the Paris Agreements.⁵³ Still, uncertainty remains about the projections from climate models following this scenario, especially for precipitation projections at the regional scales.⁷⁸ To take into account such uncertainties and capture their magnitude, nine different climate models were considered in our study. Although differing in their magnitude, outputs from computations based on all climate models converged in predicting the global trends of *Aedes* densities—i.e., a regional increase of *Ae. aegypti* densities in the continent for all scenarios and a contrast between an increase of *Ae. albopictus* densities in highlands and a decrease in lowlands.

A main source of uncertainty in density projections remained in the parameters and weather-dependent functions used to describe the mortality and transitions rates between life stages of mosquito cycles. An interesting consideration is that a similar process-based compartment model developed by Liu-Helmersson et al.²⁵ using different functions and parameters than the present study reached opposite conclusions in some parts of Southeast Asia for projections of *Ae. aegypti* densities. The roots of such discrepancies were explored here. They probably lie in important quantitative differences in temperature-dependent transition functions between the Liu-Helmersson et al. study and the present study, such as transition rates from larvae to pupae and from pupae to adult (Figure S18). Indeed, a sharp decline in transition rates used by Liu-Helmersson et al.²⁵ above 20°–22°C is consistent with their predicted decrease of adult densities in Southeast Asia lowlands, where rising temperatures are more likely to exceed the optimal temperature threshold of their model.

Such divergence in functions and outputs reveals the importance of proper parameter estimates in process-based models. Process-based models are based on solid scientific knowledge of the species biology, but confidence in such models' predictions can only come from a confidence in the underlying functions used to describe species' response to given meteorological variations. Unfortunately, there are too few observational-based studies to choose such parametrization with confidence, and these may also be spatially dependent. Given the paucity of observations, researchers rely on the current literature to implement such climate-dependent parametrization, and we advocate for more observational/lab studies to estimate how the mosquito life cycles depend on meteorological variables at regional scales across the world.

Validation

Because weather variables show great variability at the seasonal scale, the ability of our model to describe adult density response to these variables was attested to through comparison with seasonal dynamics of mosquito densities measured from field survey. Validation of spatial dynamics was not feasible here due to the inherent difficulty of gathering spatially consistent mosquito density data. Indeed, most methods used to survey mosquito abundance or density involve the use of traps to capture eggs and adults, which can be subject to spatially inconsistent sources of bias. Indeed, adult traps can only capture an unknown and variable proportion of adults in a location, whereas egg traps can be biased by local availability of breeding sites (a higher number of surrounding breeding sites

dilutes the number of adults that will lay eggs in the trap).⁷⁹ Mark-release-recapture methods are able to approximate consistently the abundance of mosquitoes in different locations^{80–83} but are very costly and time-consuming.

Field data from Phnom Penh and Vientiane were used here to estimate only seasonal variations of *Aedes* densities. In Phnom Penh, records covered only a single year of sampling and were therefore not likely to be fully representative of the seasonal variations of densities in the location. Still, seasonal dynamics of densities, although contrasted between the two species, appeared to both match with outputs from the process-based model.

Further Uses of Modeled Mosquito Densities for Vectorborne Diseases

Model outputs describing vector risk can be used in different ways to investigate how it translates into disease risk. Such process-based model outputs have indeed been used as input in dengue mechanistic transmission models.⁸⁴ Temporally variable indices of adult density, for instance those modeled from historical observed gridded climate data (e.g., from the Worldclim data set), could also be used in statistical models as an independent covariate to build better disease predictive models when long-term data from density surveys are not available. Outputs from large-scale process-based models of *Ae. aegypti* density have indeed been shown to correlate with local dengue fever caseload.⁸⁵ Yet, causal relationships between vector density and disease risk are not completely apprehended for diseases like dengue fever^{11,86} as a result of a lack of long-term reliable longitudinal entomological survey data.^{11,13} In such contexts, process-based model outputs can be useful as proxies to investigate empirical relationships between vector density and recorded disease dynamics.

Conclusion

This work brings new insights about the benefits and limitations of process-based approaches for the modeling of mosquito densities and provides a new tool for investigating the climate dependency of mosquito-borne diseases dynamics. Most important, these findings carry further evidence that climate changes that are human in origin will impact ecosystems and, in turn, public health by highlighting the threat of a rise in densities of a potent vector for numerous infectious diseases in Southeast Asia for the coming 21st century. We show that reductions of greenhouse gas emissions following strictly the Paris Agreements, although unlikely at the date of the present study, would have a limited impact on this increase in vector risk.

Acknowledgments

This work was funded by the Agence Française de Développement (AFD), in the framework of the ECOMORE II project (<http://ecomore.org/>).

Model outputs are available for download at <https://doi.org/10.23708/NYX0NV>.

References

1. Bhatt S, Gething PW, Brady OJ, Messina JP, Farlow AW, Moyes CL, et al. 2013. The global distribution and burden of dengue. *Nature* 496(7446):504–507, PMID: 23563266, <https://doi.org/10.1038/nature12060>.
2. Petersen LR, Jamieson DJ, Powers AM, Honein MA. 2016. Zika virus. *N Engl J Med* 374(16):1552–1563, PMID: 27028561, <https://doi.org/10.1056/NEJMra1602113>.
3. Caglioti C, Lalle E, Castilletti C, Carletti F, Capobianchi MR, Bordini L, et al. 2013. Chikungunya virus infection: an overview. *New Microbiol* 36(3):211–227, PMID: 23912863.
4. LaBeaud AD, Bashir F, King CH. 2011. Measuring the burden of arboviral diseases: the spectrum of morbidity and mortality from four prevalent infections. *Popul Health Metr* 9(1):1, PMID: 21219615.

5. WHO (World Health Organization). 2019. Dengue and Severe Dengue. <https://www.who.int/news-room/fact-sheets/detail/dengue-and-severe-dengue> [accessed 1 March 2021].
6. Morrison AC, Zielinski-Gutierrez E, Scott TW, Rosenberg R. 2008. Defining challenges and proposing solutions for control of the virus vector *Aedes aegypti*. *PLoS Med* 5(3):e68, PMID: 18351798, <https://doi.org/10.1371/journal.pmed.0050068>.
7. Ooi E-E, Goh K-T, Gubler DJ. 2006. Dengue prevention and 35 years of vector control in Singapore. *Emerg Infect Dis* 12(6):887–893, PMID: 16707042, <https://doi.org/10.3201/eid1206.051210>.
8. Vega-Rúa A, Lourenço-de-Oliveira R, Mousson L, Vazeille M, Fuchs S, Yébakima A, et al. 2015. Chikungunya virus transmission potential by local aedes mosquitoes in the Americas and Europe. *PLoS Negl Trop Dis* 9(5): e0003780, PMID: 25993633, <https://doi.org/10.1371/journal.pntd.0003780>.
9. Rodríguez-Morales AJ. 2015. Zika: the new arbovirus threat for Latin America. *J Infect Dev Ctries* 9(6):684–685, PMID: 26142684, <https://doi.org/10.3855/jidc.7230>.
10. Kramer LD, Ciota AT. 2015. Dissecting vectorial capacity for mosquito-borne viruses. *Curr Opin Virol* 15:112–118, PMID: 26569343, <https://doi.org/10.1016/j.coviro.2015.10.003>.
11. Bowman LR, Runge-Ranzinger S, McCall PJ. 2014. Assessing the relationship between vector indices and dengue transmission: a systematic review of the evidence. *PLoS Negl Trop Dis* 8(5):e2848, PMID: 24810901, <https://doi.org/10.1371/journal.pntd.0002848>.
12. Barrera R, Amador M, MacKay AJ. 2011. Population dynamics of *Aedes aegypti* and dengue as influenced by weather and human behavior in San Juan, Puerto Rico. *PLoS Negl Trop Dis* 5(12):e1378, PMID: 22206021, <https://doi.org/10.1371/journal.pntd.0001378>.
13. Cromwell EA, Stoddard ST, Barker CM, Van Rie A, Messer WB, Meshnick SR, et al. 2017. The relationship between entomological indicators of *Aedes aegypti* abundance and dengue virus infection. *PLoS Negl Trop Dis* 11(3): e0005429, PMID: 28333938, <https://doi.org/10.1371/journal.pntd.0005429>.
14. Chadee DD. 2009. Dengue cases and *Aedes aegypti* indices in Trinidad, West Indies. *Acta Trop* 112(2):174–180, PMID: 19632189, <https://doi.org/10.1016/j.actatropica.2009.07.017>.
15. Rodríguez-Figueroa L, Rigau-Perez JG, Suarez EL, Reiter P. 1995. Risk factors for dengue infection during an outbreak in Yanes, Puerto Rico in 1991. *Am J Trop Med Hyg* 52(6):496–502, PMID: 7611553, <https://doi.org/10.4269/ajtmh.1995.52.496>.
16. Sedda L, Taylor BM, Eiras AE, Marques JT, Dillon RJ. 2020. Using the intrinsic growth rate of the mosquito population improves spatio-temporal dengue risk estimation. *Acta Trop* 208:105519, PMID: 32389450, <https://doi.org/10.1016/j.actatropica.2020.105519>.
17. Marinho RA, Beserra EB, Bezerra-Gusmão MA, Porto V. D S, Olinda RA, Dos Santos CAC, et al. 2016. Effects of temperature on the life cycle, expansion, and dispersion of *Aedes aegypti* (Diptera: Culicidae) in three cities in Paraíba, Brazil. *J Vector Ecol* 41(1):1–10, PMID: 27232118, <https://doi.org/10.1111/jvec.12187>.
18. Kweka EJ, Baraka V, Mathias L, Mwang'onde B, Baraka G, Lyaruu L, et al. 2018. Ecology of *Aedes* Mosquitoes, The Major Vectors of Arboviruses in Human Population. In: *Dengue Fever: A Resilient Threat in the Face of Innovation*. Falcón-Lezama JA, Betancourt-Cravioto M, Tapia-Conyer R, eds. <https://doi.org/10.5772/intechopen.81439>.
19. Kraemer MUG, Reiner RC, Brady OJ, Messina JP, Gilbert M, Pigott DM, et al. 2019. Past and future spread of the arbovirus vectors *Aedes aegypti* and *Aedes albopictus*. *Nat Microbiol* 4(5):854–863, PMID: 30833735, <https://doi.org/10.1038/s41564-019-0376-y>.
20. Kraemer MUG, Sinka ME, Duda KA, Mylne A, Shearer FM, Brady OJ, et al. 2015. The global compendium of *Aedes aegypti* and *Ae. albopictus* occurrence. *Sci Data* 2:150035, PMID: 26175912, <https://doi.org/10.1038/sdata.2015.35>.
21. Ducheyne E, Tran Minh NN, Haddad N, Bryssinckx W, Buliva E, Simard F, et al. 2018. Current and future distribution of *Aedes aegypti* and *Aedes albopictus* (Diptera: Culicidae) in WHO Eastern Mediterranean region. *Int J Health Geogr* 17(1):4, PMID: 29444675, <https://doi.org/10.1186/s12942-018-0125-0>.
22. Ding F, Fu J, Jiang D, Hao M, Lin G. 2018. Mapping the spatial distribution of *Aedes aegypti* and *Aedes albopictus*. *Acta Trop* 178:155–162, PMID: 29191515, <https://doi.org/10.1016/j.actatropica.2017.11.020>.
23. Focks DA, Haile DG, Daniels E, Mount GA. 1993. Dynamic life table model for *Aedes aegypti* (Diptera: Culicidae): analysis of the literature and model development. *J Med Entomol* 30(6):1003–1017, PMID: 8271242, <https://doi.org/10.1093/jmedent/30.6.1003>.
24. Hopp MJ, Foley JA. 2001. Global-scale relationships between climate and the dengue fever vector, *Aedes aegypti*. *Clim Change* 48(2/3):441–463, <https://doi.org/10.1023/A:1010717502442>.
25. Liu-Helmersson J, Brännström Å, Sewe MO, Semenza JC, Rocklöv J. 2019. Estimating past, present, and future trends in the global distribution and abundance of the arbovirus vector *Aedes aegypti* under climate change scenarios. *Front Public Health* 7:148, PMID: 31249824, <https://doi.org/10.3389/fpubh.2019.00148>.
26. Cattarino L, Rodríguez-Barraquer I, Imai N, Cummings DAT, Ferguson NM. 2020. Mapping global variation in dengue transmission intensity. *Sci Transl Med* 12(528), <https://doi.org/10.1126/scitranslmed.aax4144>.
27. Lugito NPH. 2017. Trends of dengue disease epidemiology. *Virology* (Auckl) 8:1178122X17695836, PMID: 28579763, <https://doi.org/10.1177/1178122X17695836>.
28. Boyer S, Lopes S, Prasetyo D, Hustedt J, Sarady AS, Doum D, et al. 2018. Resistance of *Aedes aegypti* (Diptera: Culicidae) populations to deltamethrin, permethrin, and temephos in Cambodia. *Asia Pac J Public Health* 30(2):158–166, PMID: 29502428, <https://doi.org/10.1177/1010539517753876>.
29. Marcombe S, Fustec B, Cattel J, Chonephetsarath S, Thammavong P, Phommavanh N, et al. 2019. Distribution of insecticide resistance and mechanisms involved in the arbovirus vector *Aedes aegypti* in Laos and implication for vector control. *PLOS Negl Trop Dis* 13(12):e0007852, PMID: 31830027, <https://doi.org/10.1371/journal.pntd.0007852>.
30. Calvez E, Pommelet V, Somlor S, Pompon J, Viengphouthong S, Bounmany P, et al. 2020. Trends of the dengue serotype-4 circulation with epidemiological, phylogenetic, and entomological insights in Lao PDR between 2015 and 2019. *Pathogens* 9(9):728, <https://doi.org/10.3390/pathogens9090728>.
31. Eyring V, Bony S, Meehl GA, Senior CA, Stevens B, Stouffer RJ, et al. 2016. Overview of the coupled model intercomparison project phase 6 (CMIP6) experimental design and organization. *Geosci Model Dev* 9(5):1937–1958, <https://doi.org/10.5194/gmd-9-1937-2016>.
32. Cailly P, Tran A, Balenghien T, L'Ambert G, Toty C, Ezanno P, et al. 2012. A climate-driven abundance model to assess mosquito control strategies. *Ecological Modelling* 227:7–17, <https://doi.org/10.1016/j.ecolmodel.2011.10.027>.
33. Tran A, L'Ambert G, Lacour G, Benoît R, Demarchi M, Cros M, et al. 2013. A rainfall- and temperature-driven abundance model for *Aedes albopictus* populations. *Int J Environ Res Public Health* 10(5):1698–1719, PMID: 23624579, <https://doi.org/10.3390/ijerph10051698>.
34. Tran A, Mangeas M, Demarchi M, Roux E, Degenne P, Haramboure M, et al. 2020. Complementarity of empirical and process-based approaches to modelling mosquito population dynamics with *Aedes albopictus* as an example—application to the development of an operational mapping tool of vector populations. *PLoS One* 15(1):e0227407, PMID: 31951601, <https://doi.org/10.1371/journal.pone.0227407>.
35. Delatte H, Gimonneau G, Triboire A, Fontenille D. 2009. Influence of temperature on immature development, survival, longevity, fecundity, and gonotrophic cycles of *Aedes albopictus*, vector of chikungunya and dengue in the Indian Ocean. *J Med Entomol* 46(1):33–41, PMID: 19198515, <https://doi.org/10.1603/033.046.0105>.
36. Dieng H, Rahman GMS, Abu Hassan A, Che Salmah MR, Satho T, Miaka F, et al. 2012. The effects of simulated rainfall on immature population dynamics of *Aedes albopictus* and female oviposition. *Int J Biometeorol* 56(1):113–120, PMID: 21267602, <https://doi.org/10.1007/s00484-011-0402-0>.
37. Magori K, Legros M, Puente ME, Focks DA, Scott TW, Lloyd AL, et al. 2009. Skeeter buster: a stochastic, spatially explicit modeling tool for studying *Aedes aegypti* population replacement and population suppression strategies. *PLoS Negl Trop Dis* 3(9):e508, PMID: 19721700, <https://doi.org/10.1371/journal.pntd.0000508>.
38. Xin X, Wu T, Shi X, Zhang F, Li J, Chu M, et al. 2019. BCC BCC-CSM2MR model output prepared for CMIP6 ScenarioMIP ssp370. Version 20200310. Earth System Grid Federation. <https://doi.org/10.22033/ESGF/CMIP6.3035>.
39. Voldoire A. 2019. CNRM-CERFACS CNRM-CM6-1 model output prepared for CMIP6 ScenarioMIP ssp370. Version 20200310. Earth System Grid Federation. <https://doi.org/10.22033/ESGF/CMIP6.4197>.
40. Voldoire A. 2019. CNRM-CERFACS CNRM-ESM2-1 model output prepared for CMIP6 ScenarioMIP ssp370. Version 20200310. Earth System Grid Federation. <https://doi.org/10.22033/ESGF/CMIP6.4199>.
41. Swart NC, Cole JNS, Kharin VV, Lazare M, Scinocca JF, Gillett NP, et al. 2019. CCCma CanESM5 model output prepared for CMIP6 ScenarioMIP ssp370. Version 20200310. Earth System Grid Federation. <https://doi.org/10.22033/ESGF/CMIP6.3690>.
42. John JG, Blanton C, McHugh C, Radhakrishnan A, Rand K, Vahlenkamp H, et al. 2018. NOAA-GFDL GFDL-ESM4 model output prepared for CMIP6 ScenarioMIP ssp370. Version 20200310. Earth System Grid Federation. <https://doi.org/10.22033/ESGF/CMIP6.8691>.
43. Boucher O, Denvil S, Levavasseur G, Cozic A, Caubel A, Foujols M-A, et al. 2019. IPSL IPSL-CM6A-LR model output prepared for CMIP6 ScenarioMIP ssp370. Earth System Grid Federation. <https://doi.org/10.22033/ESGF/CMIP6.5265>.
44. Tachiiri K, Abe M, Hajima T, Arakawa O, Suzuki T, Komuro Y, et al. 2019. MIROC MIROC-ES2L model output prepared for CMIP6 ScenarioMIP ssp370. Version 20200310. Earth System Grid Federation. <https://doi.org/10.22033/ESGF/CMIP6.5751>.

45. Shioyama H, Abe M, Tatebe H. 2019. MIROC MIROC6 model output prepared for CMIP6 ScenarioMIP ssp370. Version 20200310. Earth System Grid Federation. <https://doi.org/10.22033/ESGF/CMIP6.5752>.
46. Yukimoto S, Koshiro T, Kawai H, Oshima N, Yoshida K, Urakawa S, et al. 2019. MRI MRI-ESM2.0 model output prepared for CMIP6 ScenarioMIP ssp370. Version 20200310. Earth System Grid Federation. <https://doi.org/10.22033/ESGF/CMIP6.6915>.
47. Gong P, Liu H, Zhang M, Li C, Wang J, Huang H, et al. 2019. Stable classification with limited sample: transferring a 30-m resolution sample set collected in 2015 to mapping 10-m resolution global land cover in 2017. *Science Bulletin* 64(6):370–373, <https://doi.org/10.1016/j.scib.2019.03.002>.
48. Jarvis A, Reuter H, Nelson A, Guevara E. 2008. Hole-filled SRTM for the globe version 3, from the CGIAR-CSI SRTM 90m database. <https://srtm.csi.cgiar.org/srtmdata/> [accessed 10 July 2020].
49. Maquart PO, Fontenille D, Boyer S. 2021. Recent and massive invasion of aedes (Stegomyia) albopictus (Skuse, 1894) in Phnom Penh, Cambodia. *Parasit Vectors* 14(1):113, PMID: [33602318](https://doi.org/10.1186/s13071-021-04633-5), <https://doi.org/10.1186/s13071-021-04633-5>.
50. Rattanarithikul R, Harbach RE, Harrison BA, Panthasiri P, Coleman RE, Richardson JH. 2010. Illustrated keys to the mosquitoes of Thailand. VI. Tribe Aedini. *Southeast Asian J Trop Med Public Health* 41(suppl 1):1–225, PMID: [20629439](https://doi.org/10.1186/s13071-021-04633-5).
51. IPCC (Intergovernmental Panel on Climate Change). 2019 Refinement to the 2006 IPCC Guidelines for National Greenhouse Gas Inventories. <https://www.ipcc.ch/report/2019-refinement-to-the-2006-ipcc-guidelines-for-national-greenhouse-gas-inventories/> [accessed 1 March 2021].
52. The PhilPapers Foundation. Climate Change and Land: An IPCC Special Report on Climate Change, Desertification, Land Degradation, Sustainable Land Management, Food Security, and Greenhouse Gas Fluxes in Terrestrial Ecosystems. Shukla PR, Skeg J, Calvo Buendia E, Masson-Delmotte V, Pörtner H-O, Roberts DC, et al., eds. <https://philpapers.org/rec/SHUCCA-2.52> [accessed 1 March 2021].
53. UNEP (United Nations Environmental Programme). 2021. Emissions Gap Report 2021: The Heat Is On A World of Climate Promises Not Yet Delivered. <https://wedocs.unep.org/20.500.11822/36990> [accessed 1 March 2021].
54. Morin CW, Comrie AC, Ernst K. 2013. Climate and dengue transmission: evidence and implications. *Environ Health Perspect* 121(11–12):1264–1272, PMID: [24058050](https://doi.org/10.1289/ehp.1306556), <https://doi.org/10.1289/ehp.1306556>.
55. Yang HM, Macoris MLG, Galvani KC, Andrighetti MTM, Wanderley DMV. 2009. Assessing the effects of temperature on the population of Aedes aegypti, the vector of dengue. *Epidemiol Infect* 137(8):1188–1202, PMID: [19192322](https://doi.org/10.1017/S0950268809002040), <https://doi.org/10.1017/S0950268809002040>.
56. Watts DM, Burke DS, Harrison BA, Whitmore RE, Nisalak A. 1987. Effect of temperature on the vector efficiency of Aedes aegypti for dengue 2 virus. *Am J Trop Med Hyg* 36(1):143–152, PMID: [3812879](https://doi.org/10.4269/ajtmh.1987.36.143), <https://doi.org/10.4269/ajtmh.1987.36.143>.
57. Brady OJ, Golding N, Pigott DM, Kraemer MUG, Messina JP, Reiner RC, et al. 2014. Global temperature constraints on Aedes aegypti and Ae. albopictus persistence and competence for dengue virus transmission. *Parasit Vectors* 7:338, PMID: [25052008](https://doi.org/10.1186/1756-3305-7-338), <https://doi.org/10.1186/1756-3305-7-338>.
58. Mordecai EA, Caldwell JM, Grossman MK, Lippi CA, Johnson LR, Neira M, et al. 2019. Thermal biology of mosquito-borne disease. *Ecol Lett* 22(10):1690–1708, PMID: [31286630](https://doi.org/10.1111/ele.13335), <https://doi.org/10.1111/ele.13335>.
59. Smith DL, Battle KE, Hay SI, Barker CM, Scott TW, McKenzie FE, et al. 2012. Ross, Macdonald, and a theory for the dynamics and control of mosquito-transmitted pathogens. *PLoS Pathog* 8(4):e1002588, PMID: [22496640](https://doi.org/10.1371/journal.ppat.1002588), <https://doi.org/10.1371/journal.ppat.1002588>.
60. Ryan SJ, Carlson CJ, Mordecai EA, Johnson LR. 2019. Global expansion and redistribution of aedes-borne virus transmission risk with climate change. *PLoS Negl Trop Dis* 13(3):e0007213, PMID: [30921321](https://doi.org/10.1371/journal.pntd.0007213), <https://doi.org/10.1371/journal.pntd.0007213>.
61. Messina JP, Brady OJ, Golding N, Kraemer MUG, Wint GRW, Ray SE, et al. 2019. The current and future global distribution and population at risk of dengue. *Nat Microbiol* 4(9):1508–1515, PMID: [31182801](https://doi.org/10.1038/s41564-019-0476-8), <https://doi.org/10.1038/s41564-019-0476-8>.
62. Equihua M, Ibáñez-Bernal S, Benítez G, Estrada-Contreras I, Sandoval-Ruiz CA, Mendoza-Palmero FS, et al. 2017. Establishment of Aedes aegypti (L.) in mountainous regions in Mexico: increasing number of population at risk of mosquito-borne disease and future climate conditions. *Acta Trop* 166:316–327, PMID: [27863974](https://doi.org/10.1016/j.actatropica.2016.11.014), <https://doi.org/10.1016/j.actatropica.2016.11.014>.
63. Acharya B, Cao C, Xu M, Khanal L, Naeem S, Pandit S, et al. 2018. Present and future of dengue fever in Nepal: mapping climatic suitability by ecological niche model. *Int J Environ Res Public Health* 15(2):187, <https://doi.org/10.3390/ijerph15020187>.
64. Juliano SA, Lounibos LP, O'Meara GF. 2004. A field test for competitive effects of Aedes albopictus on A. aegypti in South Florida: differences between sites of coexistence and exclusion? *Oecologia* 139(4):583–593, PMID: [15024640](https://doi.org/10.1007/s00442-004-1532-4), <https://doi.org/10.1007/s00442-004-1532-4>.
65. Murrell EG, Juliano SA. 2008. Detritus type alters the outcome of interspecific competition between Aedes aegypti and Aedes albopictus (Diptera: Culicidae). *J Med Entomol* 45(3):375–383, PMID: [18533429](https://doi.org/10.1093/jmedent/45.3.375), <https://doi.org/10.1093/jmedent/45.3.375>.
66. Abilio AP, Abudasse G, Kampango A, Candrinho B, Saito S, Luciano J, et al. 2018. Distribution and breeding sites of Aedes aegypti and Aedes albopictus in 32 urban/peri-urban districts of Mozambique: implication for assessing the risk of arbovirus outbreaks. *PLoS Negl Trop Dis* 12(9):e0006692, PMID: [30208017](https://doi.org/10.1371/journal.pntd.0006692), <https://doi.org/10.1371/journal.pntd.0006692>.
67. Chareonviriyaphap T, Akranakul P, Nattanomsak S, Huntamai S. 2003. Larval habitats and distribution patterns of Aedes aegypti (Linnaeus) and Aedes albopictus (Skuse), in Thailand. *Southeast Asian J Trop Med Public Health* 34(3):529–535, PMID: [15115122](https://doi.org/10.1186/s13071-021-04633-5).
68. Cunze S, Kochmann J, Koch LK, Klimpel S. 2018. Niche conservatism of Aedes albopictus and Aedes aegypti - two mosquito species with different invasion histories. *Sci Rep* 8(1):7733, PMID: [29769552](https://doi.org/10.1038/s41598-018-26092-2), <https://doi.org/10.1038/s41598-018-26092-2>.
69. Arunachalam N, Tana S, Espino F, Kittayapong P, Abeyewickreme W, Wai KT, et al. 2010. Eco-bio-social determinants of dengue vector breeding: a multi-country study in urban and periurban Asia. *Bull World Health Organ* 88(3):173–184, PMID: [20428384](https://doi.org/10.2471/BLT.09.067892), <https://doi.org/10.2471/BLT.09.067892>.
70. Edillo FE, Roble ND, Li NDO. 2012. The key breeding sites by pupal survey for dengue mosquito vectors, Aedes aegypti (Linnaeus) and Aedes albopictus (Skuse), in Guba, Cebu City, Philippines. *Southeast Asian J Trop Med Public Health* 43(6):1365–1374, PMID: [23413699](https://doi.org/10.1186/s13071-021-04633-5).
71. Rao BB, Hari Kumar P, Jayakrishnan T, George B. 2011. Characteristics of Aedes (Stegomyia) albopictus Skuse (Diptera: Culicidae) breeding sites. *Southeast Asian J Trop Med Public Health* 42(5):1077–1082, PMID: [23413699](https://doi.org/10.1186/s13071-021-04633-5).
72. Huang K, Li X, Liu X, Seto KC. 2019. Projecting global urban land expansion and heat island intensification through 2050. *Environ Res Lett* 14(11):114037, <https://doi.org/10.1088/1748-9326/ab4b71>.
73. Tippelt L, Werner D, Kampen H. 2019. Tolerance of three Aedes albopictus strains (Diptera: Culicidae) from different geographical origins towards winter temperatures under field conditions in northern Germany. *PLoS One* 14(7):e0219553, PMID: [31310645](https://doi.org/10.1371/journal.pone.0219553), <https://doi.org/10.1371/journal.pone.0219553>.
74. Tippelt L, Werner D, Kampen H. 2020. Low temperature tolerance of three Aedes albopictus strains (Diptera: Culicidae) under constant and fluctuating temperature scenarios. *Parasit Vectors* 13(1):587, PMID: [33225979](https://doi.org/10.1186/s13071-020-04386-7), <https://doi.org/10.1186/s13071-020-04386-7>.
75. Kamimura K, Matsuse IT, Takahashi H, Komukai J, Fukuda T, Suzuki K, et al. 2002. Effect of temperature on the development of Aedes aegypti and Aedes albopictus. *Med Entomol Zool* 53(1):53–58, https://doi.org/10.7601/mez.53.53_1.
76. Sherpa S, Blum MGB, Després L. 2019. Cold adaptation in the Asian tiger mosquito's native range precedes its invasion success in temperate regions. *Evolution* 73(9):1793–1808, PMID: [31313825](https://doi.org/10.1111/evo.13801), <https://doi.org/10.1111/evo.13801>.
77. Goubert C, Henri H, Minard G, Valiente Moro C, Mavingui P, Vieira C, et al. 2017. High-throughput sequencing of transposable element insertions suggests adaptive evolution of the invasive Asian tiger mosquito towards temperate environments. *Mol Ecol* 26(15):3968–3981, PMID: [28517033](https://doi.org/10.1111/mec.14184), <https://doi.org/10.1111/mec.14184>.
78. Intergovernmental Panel on Climate Change. 2021. Climate Change 2021: The Physical Science Basis. Contribution of Working Group I to the Sixth Assessment Report of the Intergovernmental Panel on Climate Change. Cambridge, UK: Cambridge University Press.
79. Focks DA, UNDP (United Nations Development Programme)/World Bank/WHO Special Programme for Research and Training in Tropical Diseases. 2004. A Review of Entomological Sampling Methods and Indicators for Dengue Vectors, <https://apps.who.int/iris/handle/10665/68575> [accessed 1 March 2021].
80. Maciel-de-Freitas R, Eiras AE, Lourenço-de-Oliveira R. 2008. Calculating the survival rate and estimated population density of gravid Aedes aegypti (Diptera, Culicidae) in Rio de Janeiro. *Cad Saúde Pública* 24(12):2747–2754, <https://doi.org/10.1590/S0102-311X2008001200003>.
81. Mercer DR, Marie J, Bossin H, Faarua M, Tetuanui A, Sang MC, et al. 2012. Estimation of population size and dispersal of Aedes polynesiensis on Toamaro motu, French Polynesia. *J Med Entomol* 49(5):971–980, PMID: [23025176](https://doi.org/10.1603/me11234), <https://doi.org/10.1603/me11234>.
82. Neira M, Lacroix R, Cáceres L, Kaiser PE, Young J, Pineda L, et al. 2014. Estimation of Aedes aegypti (Diptera: Culicidae) population size and adult male survival in an urban area in Panama. *Mem Inst Oswaldo Cruz* 109(7):879–886, PMID: [25410991](https://doi.org/10.1590/0074-0276140136), <https://doi.org/10.1590/0074-0276140136>.
83. Villela DAM, Codeço CT, Figueiredo F, Garcia GA, Maciel-de-Freitas R, Struchiner CJ, et al. 2015. A Bayesian hierarchical model for estimation of

- abundance and spatial density of *Aedes aegypti*. PLoS One 10(4):e0123794, PMID: [25906323](https://pubmed.ncbi.nlm.nih.gov/25906323/), <https://doi.org/10.1371/journal.pone.0123794>.
84. Focks DA, Daniels E, Haile DG, Keesling JE. 1995. A simulation model of the epidemiology of urban dengue fever: literature analysis, model development, preliminary validation, and samples of simulation results. Am J Trop Med Hyg 53(5):489–506, PMID: [7485707](https://pubmed.ncbi.nlm.nih.gov/7485707/), <https://doi.org/10.4269/ajtmh.1995.53.489>.
 85. Hopp M, Foley J. 2003. Worldwide fluctuations in dengue fever cases related to climate variability. Clim Res 25:85–94, <https://doi.org/10.3354/cr025085>.
 86. Scott TW, Morrison A. 2004. Chapter 14: *Aedes aegypti* density and the risk of dengue-virus transmission. In: *Ecological Aspects for Application of Genetically Modified Mosquitoes*, vol. 2. Takken W, Scott TW, eds. Cham, Switzerland: Springer Frontis Series, 187–206.